Absolute Luminosity Measurement with the H1 detector using Quasi-Real QED Compton Process

V.F.Andreev

Lebedev Physical Institute, Moscow

1. Introduction

In general the absolute luminosity can be determined from the following expression

$$L = \frac{R}{\sigma A \varepsilon}$$

where L - absolute luminosity, σ - cross section of the process used for the absolute luminosity measurement (in our case it is quasi-real QED Compton process), A - geometrical acceptance for this process, ϵ - trigger efficiency and R - measured rate of events. The systematic error comes from the following sources:

a) accuracy of the theoretical description for selected process,
b) uncertainty of the geometrical acceptance,
c) uncertainty of the trigger efficiency,
d) uncertainty of the Monte Carlo simulation,
e) also uncertainty comes from different background processes.

2. Quasi-Real QED Compton Process

As it was shown by A.Courau et al. [1] it possible to use the quasi-real QED Compton process for the absolute luminosity measurement at H1 detector. The reaction $ep \to e\gamma X$ corresponds to the following diagram

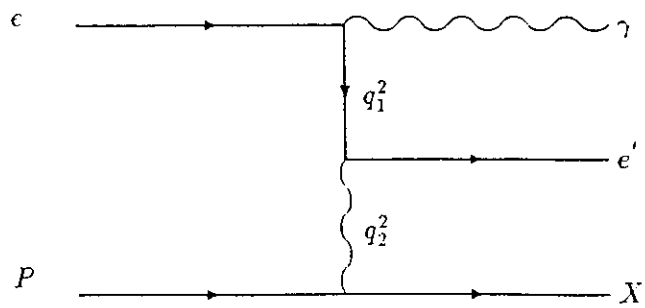

where $q_2^2 \to 0$ and $q_1^2 \to finite$. Since the hadronic system is strongly boosted in the forward direction one can mainly observe only the electron and the photon in the H1 detector. The Monte Carlo generator for the quasi-real QED Compton process is available now [2] and was

used in our investigations. More details about Monte Carlo generator one can find elsewhere [2]. Using this generator $\sim$ 70.000 events were generated with the following conditions:

- E_e = 26.7 GeV - the incident electron energy,
- E_p = 820.0 GeV - the incident proton energy,
- $3.6^o \leq \theta_{e'}, \theta_\gamma \leq 176^o$ - the angular range of the scattered electron and photon,
- $E_{e'}, E_\gamma \geq 2\ GeV$, $E_{e'}+E_\gamma \geq 20\ GeV$ - the energy cuts,
- $\pi - |\phi_{e'} - \phi_\gamma| \leq 45^o$ - the acoplanarity cut.

The total cross section of the Compton process for these experimental conditions is σ_{tot} = 2363.7 pb consisting of the elastic part σ_{el} = 1414.5 pb and the inelastic part σ_{in} = 949.2 pb. Figure 1 shows the dependence of the differential cross section $\frac{d\sigma}{d\theta}$ on the polar angle θ of the electron and the photon. The main feature of this process is the sharp angular dependence of the cross section such that almost whole cross section is within the acceptance of BEMC.

The theoretical uncertainty for the elastic channel determined by the uncertainty of the elastic proton form factors is $\sim$ 2 % . For the inelastic channel the accuracy is limited by the uncertainty of the proton structure function and is $\sim$ 10 % .

3. Geometrical acceptance

In this part the geometrical acceptance is considered. The geometry of the backward area of the H1 detector is shown in figure 2. The polar angle θ can be divided on three parts (see fig. 2): θ_1 - the lower angle boundary of BEMC ($\theta_1 \sim 155^o$), θ_2 - the upper angle boundary of CIZ ($\theta_2 \sim 170^o$), θ_3 - the upper angle boundary of BEMC ($\theta_3 \sim 176^o$). One should stress that these angles depend on the position of interaction point.

We shall consider three different cases:

a) "TRIG1" - both the electron and the photon are within acceptance of the H1 detector $3.6^o \leq \theta_{e'}, \theta_\gamma \leq \theta_3$ (this case is considered only for comparison),

b) "TRIG2" - the electron and the photon are within acceptance of the BEMC $\theta_1 \leq \theta_{e'}, \theta_\gamma \leq \theta_3$,

c) "TRIG3" - the photon within acceptance of the BEMC $\theta_1 \leq \theta_\gamma \leq \theta_3$, the electron is in BEMC and also in the tracking system of the H1 detector $\theta_1 \leq \theta_{e'} \leq \theta_2$.

The dependence of the cross section and the deviation of cross section on Z position of the interaction point is shown in figure 3 (the deviation is defined with respect σ at Z=0). Figure 4 shows the dependence of cross section and the error of cross section for the "TRIG1" case on the uncertainty of the size of interaction region (three different values of the interaction region are considered). The dependence of the error of cross section on the size and the position of interaction region is given in figure 5 (in this case 50 cm size of interaction region was taken). These pictures show that the exact knowledge of the size and the position of the interaction region is important. In general there are two possibilities to obtain this information:

- to estimate these values during the absolute luminosity measurement, which is possible only for the "TRIG3" case when the electron track can be reconstructed.
- to receive this information from other sources (the accelerator machine or during measurement of other physical processes in which the vertex is reconstructed). Of course on has to assume that the position and the size of interaction region do not change

very much during the run.

The accuracy of the vertex reconstruction with the single electron track is shown in figure 6 for the "TRIG3". $Z0$-value (z coordinate corresponding to the DCA) from the track parameters (CTKR bank) is taken as z - vertex in this case. The efficiency of the track reconstruction for the "TRIG3" is $\sim$ 100 % and the precision of the vertex reconstruction is σ=1.06 cm.

As the result the following uncertainty comes from the consideration of geometrical acceptance:

a) in the "TRIG2" case for the $\sim$ 2 % of systematic error in the cross section it is enough to know the position of the interaction region within $\binom{-10}{+5}$ cm, while for the "TRIG3" the $\binom{-3}{+3}$ cm gives $\sim$ 4 % uncertainty of the cross section,

b) the uncertainty in the size of the interaction region (this value is not so critical) for the "TRIG2" $\binom{-10}{+5}$ cm leads to $\sim$ 0.5 % systematic error in the cross section and for the "TRIG3" $\binom{-3}{+3}$ cm gives $\sim$ 0.2 % uncertainty of the cross section.

4. Trigger study

For the purpose of the trigger study 3534 quasi-real QED Compton events were simulated with H1SIM 2.06 (medium energy cuts, FLASH tracking mode, granularity for BEMC - 2 and for LAR - 3). The following conditions were chosen as the trigger:

a) NO ($MWPC - rays - T0$) signal (weak $T0$),

b) there are two or more clusters in BEMC with energy in the stack above threshold ($E_{th} = 4$ GeV),

c) total deposited energy in BEMC $E_{BEMC} \geq 10$ GeV,

d) energy in the barrel part of LAR $E_{BARR} \leq 12$ GeV,

e) forward energy $E_{FORW} \leq 20$ GeV,

f) at least 3 planes of BPC are fired (this means that there is charged particle in the BEMC region).

Two different types of trigger are considered: first - AND ($a \div e$) conditions and second - AND ($a \div f$) conditions. These trigger conditions are the same for the "TRIG2" and for the "TRIG3" and these cases can be separated only after reconstruction.

The trigger efficiency is different for the elastic and for the inelastic Compton events. The Monte Carlo generator gives the final states of the electron and the photon integrated over the final states of the proton. The next step is to estimate the part of inelastic Compton events rejected with these trigger conditions. KRONOS 1.0 generator was used [3] for simulation of inelastic Compton events and then JETSET 6.3 performed the hadronization. With KRONOS 1.0 $\sim$ 1000 inelastic Compton events were generated within the same experimental conditions, and then these events were simulated with H1SIM 2.06. As the result, the trigger efficiency for the elastic Compton events is $\sim$ 80 % and for the inelastic events is $\sim$ 60 %.

The final trigger efficiency is shown in the table 1. The trigger efficiency is determined with respect to the geometrical cross section (σ = 1962.1 pb for "TRIG2" and σ = 780.1 pb for "TRIG3" cases). In the 3-rd and 4-th lines of this table the same values are given with account of noise in BEMC.

Inefficiency of the trigger is mainly explained by the boundary effects when part of the energy is lost and also when the energy of one particle is deposited in two stacks of BEMC with almost equal energy per stack less than trigger threshold. The dependence of the trigger efficiency and the error of trigger efficiency on the uncertainty of the energy stack threshold

is shown in figure 7.

Table I. Trigger efficiency for different conditions

	Geometrical acceptance(%)	*Trigger efficiency (%)*		*Visible cross section (pb)*	
		with BPC	*without BPC*	*with BPC*	*without BPC*
TRIG2	83.3	59.7	70.4	1170.	1380.
TRIG3	32.7	72.8	74.2	570.	580.
TRIG2	83.3	61.8	71.7	1210.	1410.
TRIG3	32.7	74.0	75.5	580.	590.

One can conclude that for the 2 % level uncertainty of the trigger efficiency it is necessary to keep the stability of the trigger stack threshold within ± 0.2 *GeV* limits (5 %). Trigger efficiency for the Compton events is not very sensitive to the *LAR* energy thresholds.

A special MC simulation has shown that 10 % uncertainty of BEMC responce leads to the error of trigger efficiency of 2 %.

5. Background study

In this part the background to the quasi-real QED Compton events is discussed. First of all this is the process of Deep Inelastic Scattering (DIS) with radiative corrections when the radiative photon and the scattered electron are in the acceptance of BEMC. The radiative corrections were generated with KRONOS 1.0 using JETSET 6.3 for the hadronization of the proton. The total cross section of this process within above discribed experimental conditions is $\sigma_{tot} = 9940$ *pb*, which is in ~ 5 times more than the cross section of the Compton process. 1070 *DIS* events with radiative gammas have been generated and passed through H1SIM 2.06. The obtained result after applying of trigger conditions is shown in table 2.

Table II. Triggered cross section of DIS process with radiative photons

	Visible cross section (pb) with BPC trigger		*Visible cross section (pb) without BPC trigger*	
	TRIG2	*TRIG3*	*TRIG2*	*TRIG3*
DIS events without acoplanarity cut	550.	140.	770.	140.
DIS events with acoplanarity cut	270.	40.	450.	40.

At this level the contribution from DIS process is $\sim$ 20 % for "TRIG2" and $\sim$ 7 % for "TRIG3" cases (if acoplanarity cut is applied). Futher suppresion of this background can be done after reconstruction (for example to select events with low W_H and relatively high $(e'\gamma)$ invariant masses). An additional study is necessary in this direction.

The next step was to estimate the possible contribution from the beamwall and the beam-gas events. For this purpose the standard H1 files were used:

a) beamwall events
HERA02.MAR.QSIRON.OUTPUT01.H1SIM001 - H1SIM006 and
H1KFED.BEAMWALL.MODB.BEAMLINE.H1SIM.C001 - C002
(total statistics $\sim$ 110000 events with 1 event corresponding to $\sim 5\ Hz$),
b) beamgas events
HERA02.BEAMLINE.MODC.RUN01.PART01.H1SIM001 - H1SIM014
(total statistics $\sim$ 100000 events with 1 event corresponding to $\sim 3\ Hz$) .
All these BEAMWALL and BEAMGAS events were rejected after applying the proposed trigger cuts . Thus only upper limit can be estimated with present statistics. And this estimation gives $\leq 300\ nb$ for beamwall and $\leq 200\ nb$ for beamgas events.

6. Conclusions

The possibility of the absolute luminosity measurement is investigated using the quasi-real QED Compton process. The trigger conditions are found separating the Compton events from the background. The systematic error comes from the following sources:

- theoretical uncertainty $\sim$ 4 %,
- uncertainty of the geometrical acceptance for "TRIG2" case is $\sim$ 2 % and for "TRIG3" case is $\sim$ 4 %,
- uncertainty of trigger efficiency $\sim$ 2 %,
- uncertainty of the Monte Carlo simulation $\sim$ 2 %.

As the result the total systematic error is $\sim$ 5.5 % for the "TRIG2" with 20 % background contribution from the DIS with radiative corrections and is $\sim$ 6.5 % for the "TRIG3" case with 7 % contribution from radiative corrections.

Futher steps are to try to reduce the contribution from the background and to study some other sources of background (like soft photoproduction etc.). In order to reduce systematic error it is also necessary to separate elastic and inelastic channels of the Compton process. In principle this is possible after reconstruction .

References

[1] A.Courau, *Phys.Lett., 151B, No.5,6 (1985)469.*
A.Courau and P.Kessler, *Phys.Rev., D33, No.7(1986)2028.*

[2] A.Courau, *H1 note H1-07/91-186.*
A.Courau and et al., *H1 note H1-12/91-207.*

[3] H.Anlauf and et al., *Preprint DESY. DESY 91-100,September 1991.*

Figure Captions

Fig. 1 Dependence of the differential cross section $\frac{d\sigma}{d\theta}$ for quasi-real QED Compton process on the polar angle θ: (a) - for the electron, (b) - for the photon.

Fig. 2 Geometry of the backward area of H1 detector:
θ_1 - the lower angle boundary of BEMC ($\theta_1 \sim 155^\circ$),
θ_2 - the upper angle boundary of CIZ ($\theta_2 \sim 170^\circ$),
θ_3 - the upper angle boundary of BEMC ($\theta_3 \sim 176^\circ$).

Fig. 3 Dependence of the (a) - visible cross section and (b) - deviation of cross section of the quasi-real QED Compton process on the position of interaction point (in this picture and later +z axis is in the direction of the electron beam): solid line - for the "TRIG1", dashed line - for the "TRIG2" and dash-dotted line - for the "TRIG3" cases.

Fig. 4 Dependence of the (a) - visible cross section and (b) - error of the cross section for the "TRIG1" on the uncertainty of the size of interaction region: dashed line - the size of interaction region is 30 *cm*, solid line - 50 *cm* and dash-dotted line - 70 *cm*.

Fig. 5 Dependence of the error of cross section on the uncertainty (a) - the size and (b) - position of interaction region (50 *cm* size of interaction region was taken).

Fig. 6 (a) - the accuracy of vertex reconstruction for "TRIG3" case,
(b) - dependence of the accuracy of vertex reconstruction on the position of interaction point.

Fig. 7 Dependence of the (a) - trigger efficiency and (b) - error of trigger efficiency on the uncertainty of the stack energy threshold: dashed line - for the "TRIG2" and dash-dotted line - for the "TRIG3" cases.

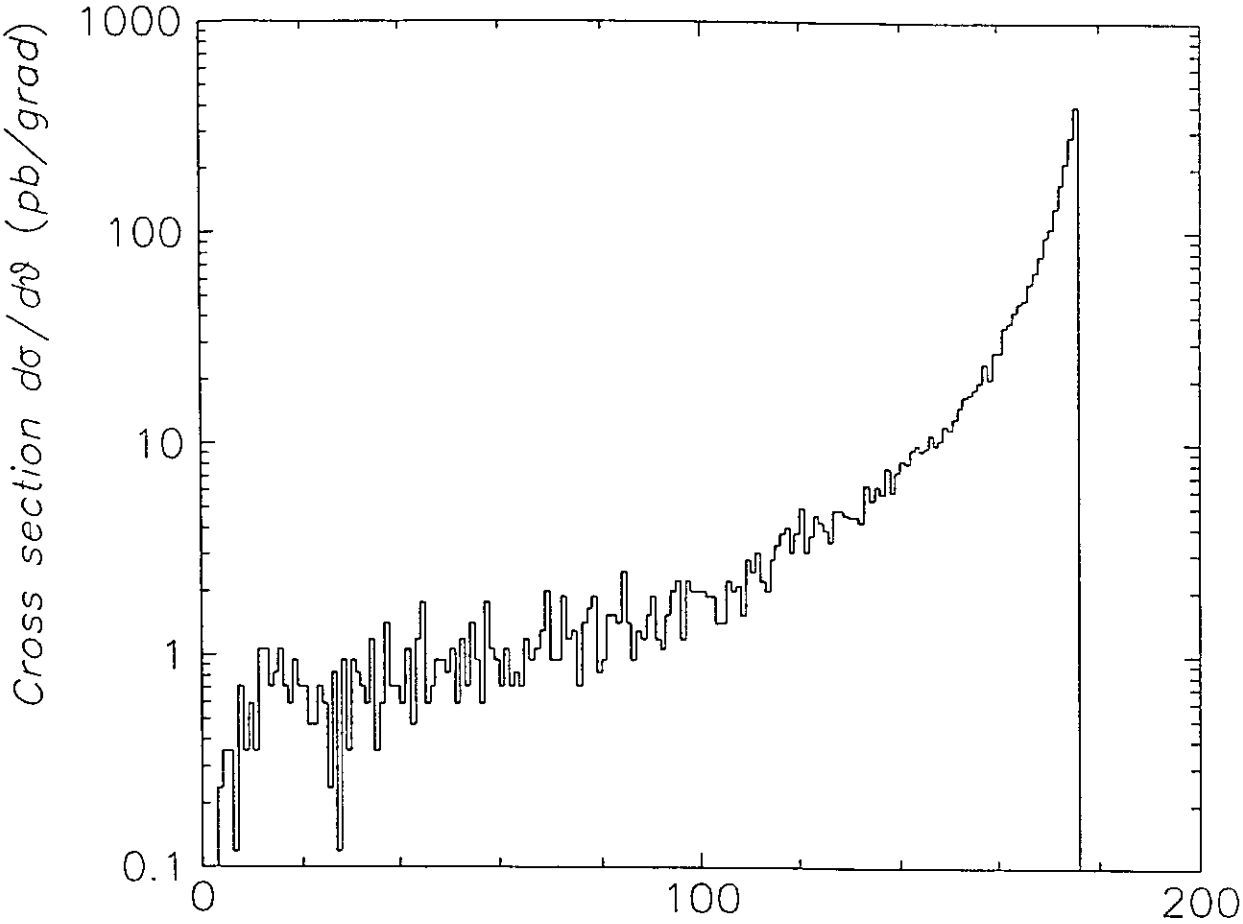

Figure 1(a)

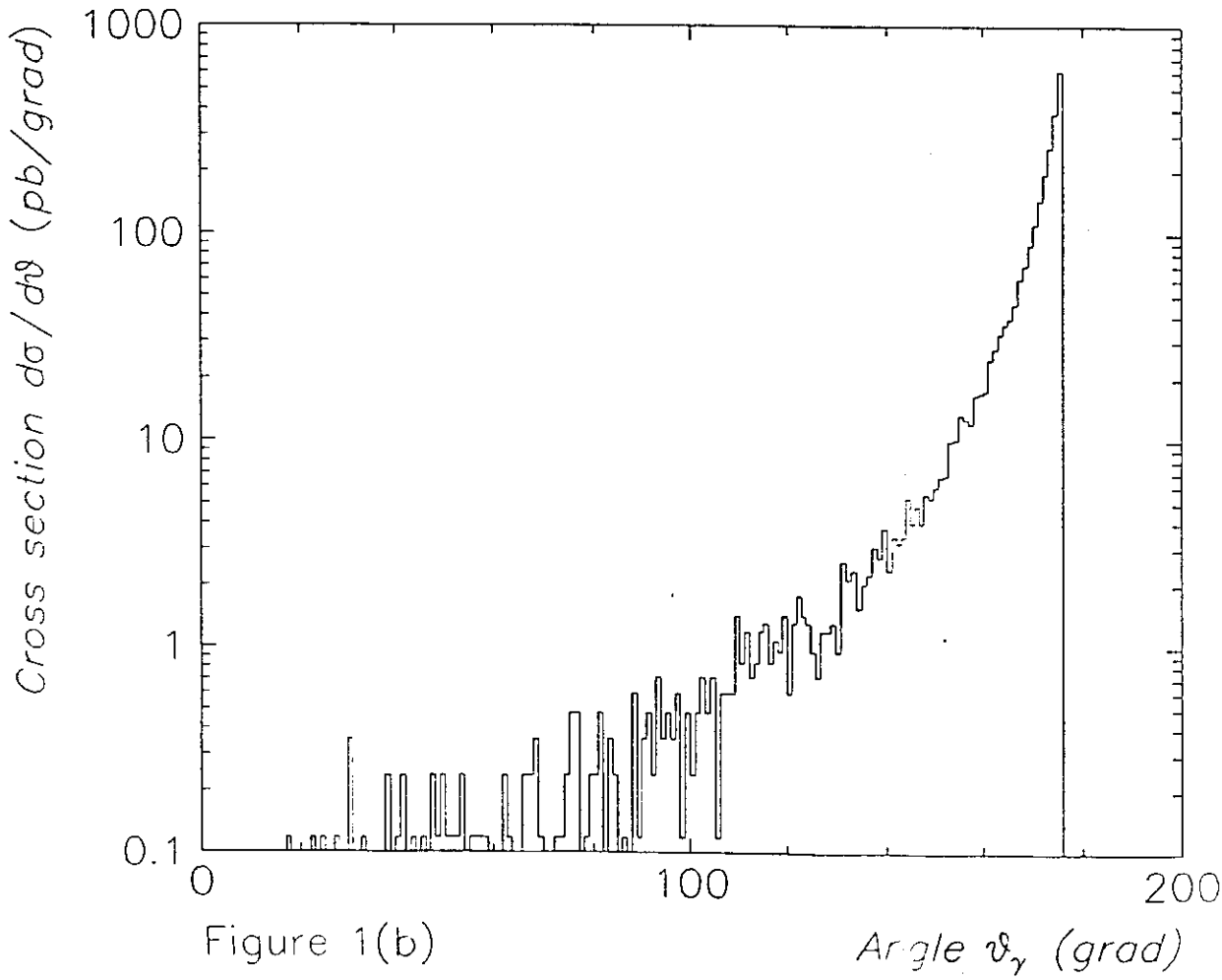

Figure 1(b)

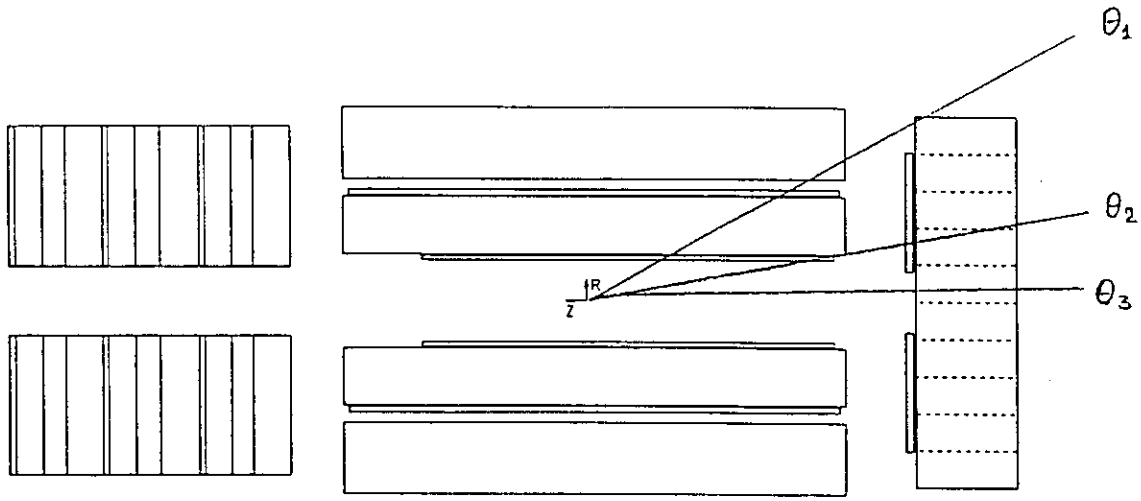

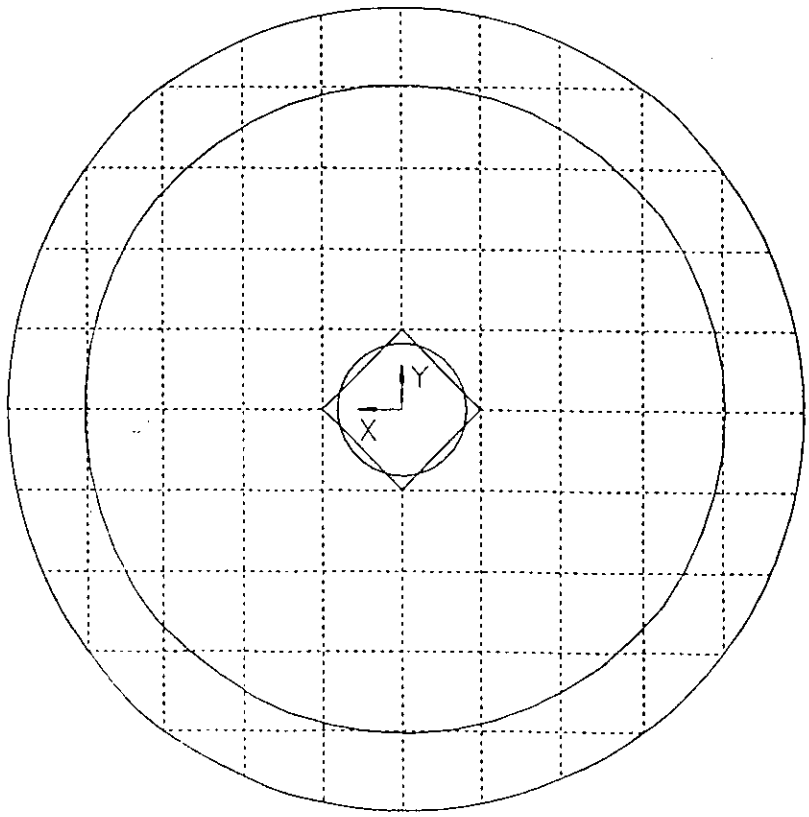

Figure 2

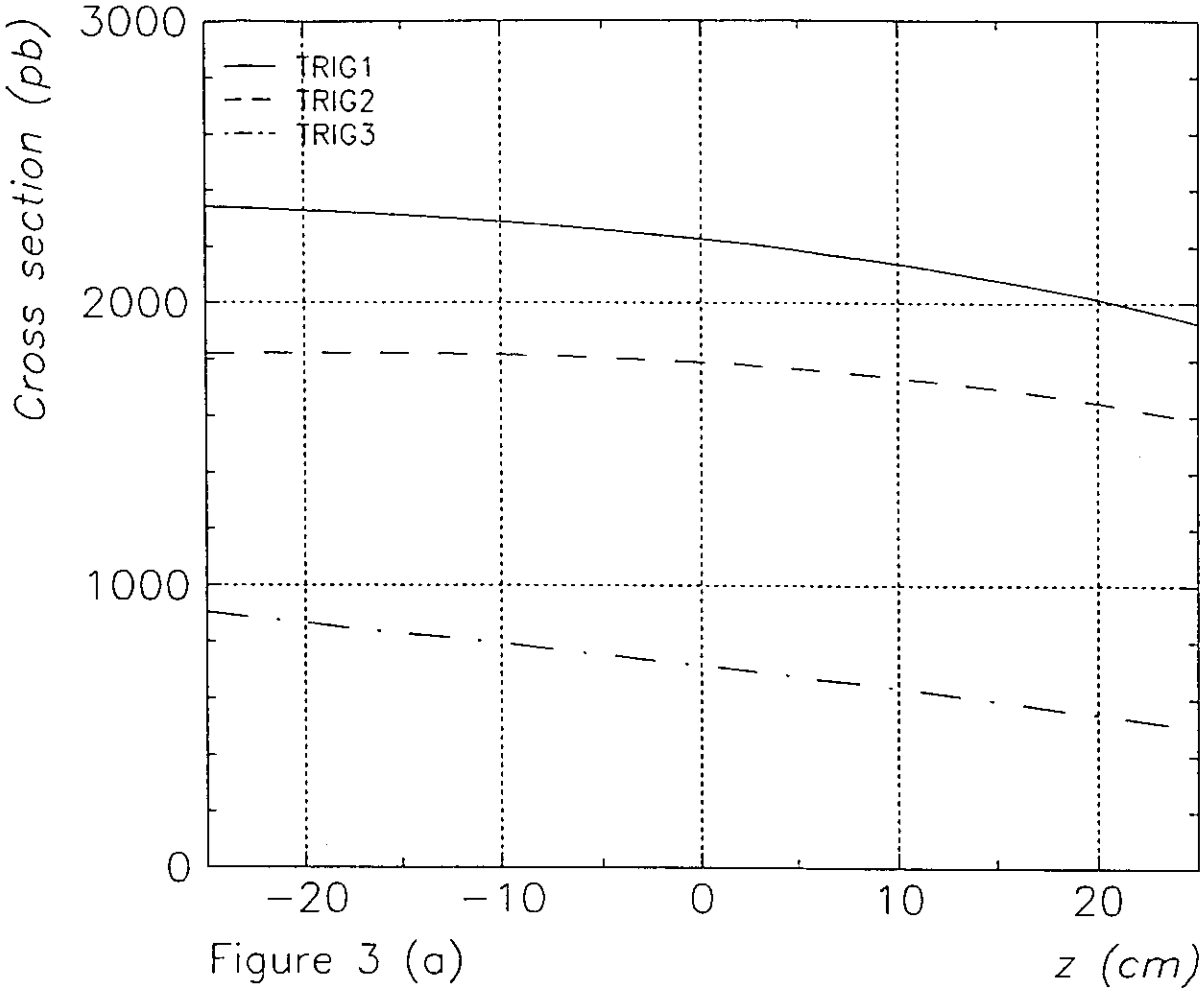

Figure 3 (a)

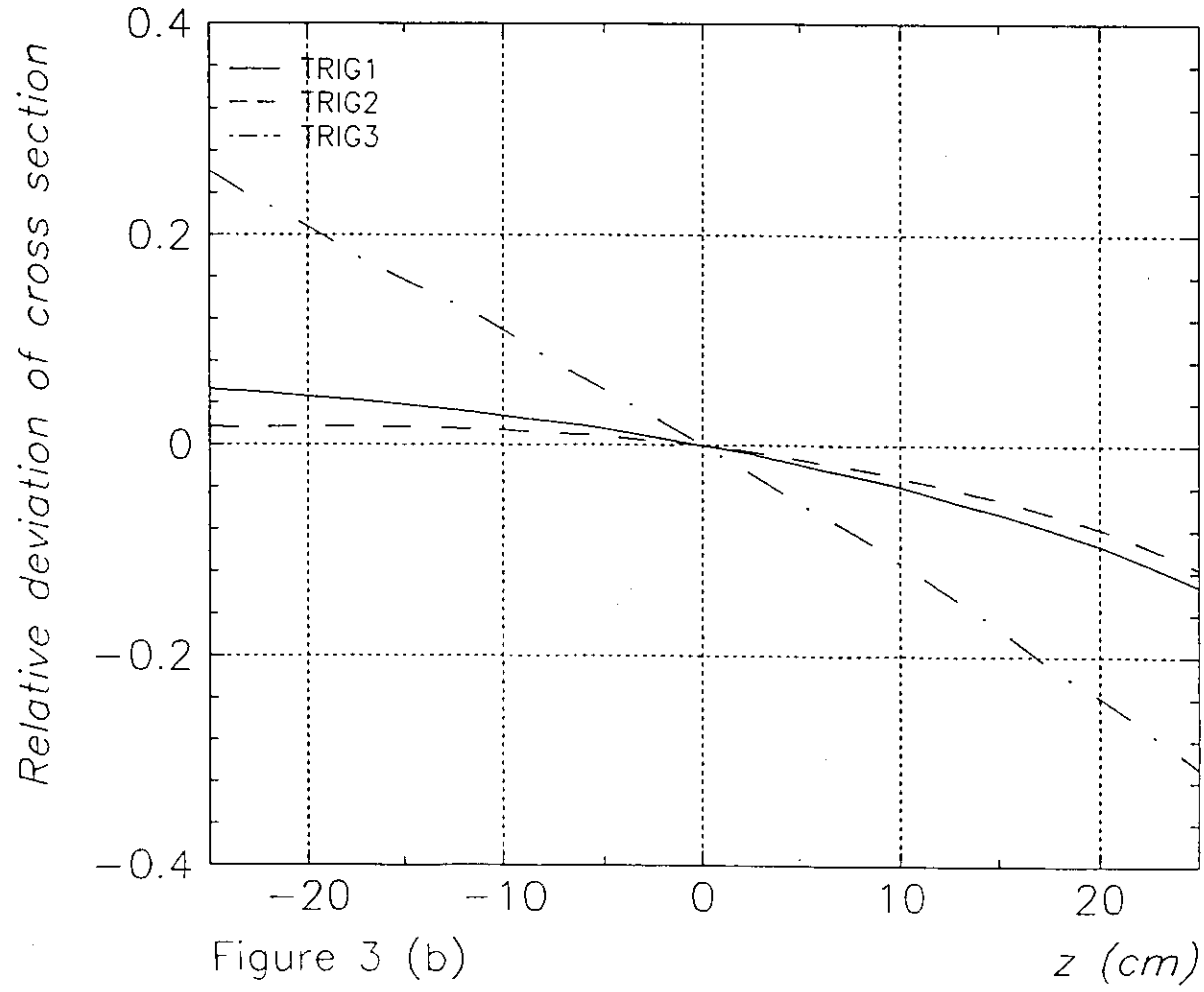

Figure 3 (b)

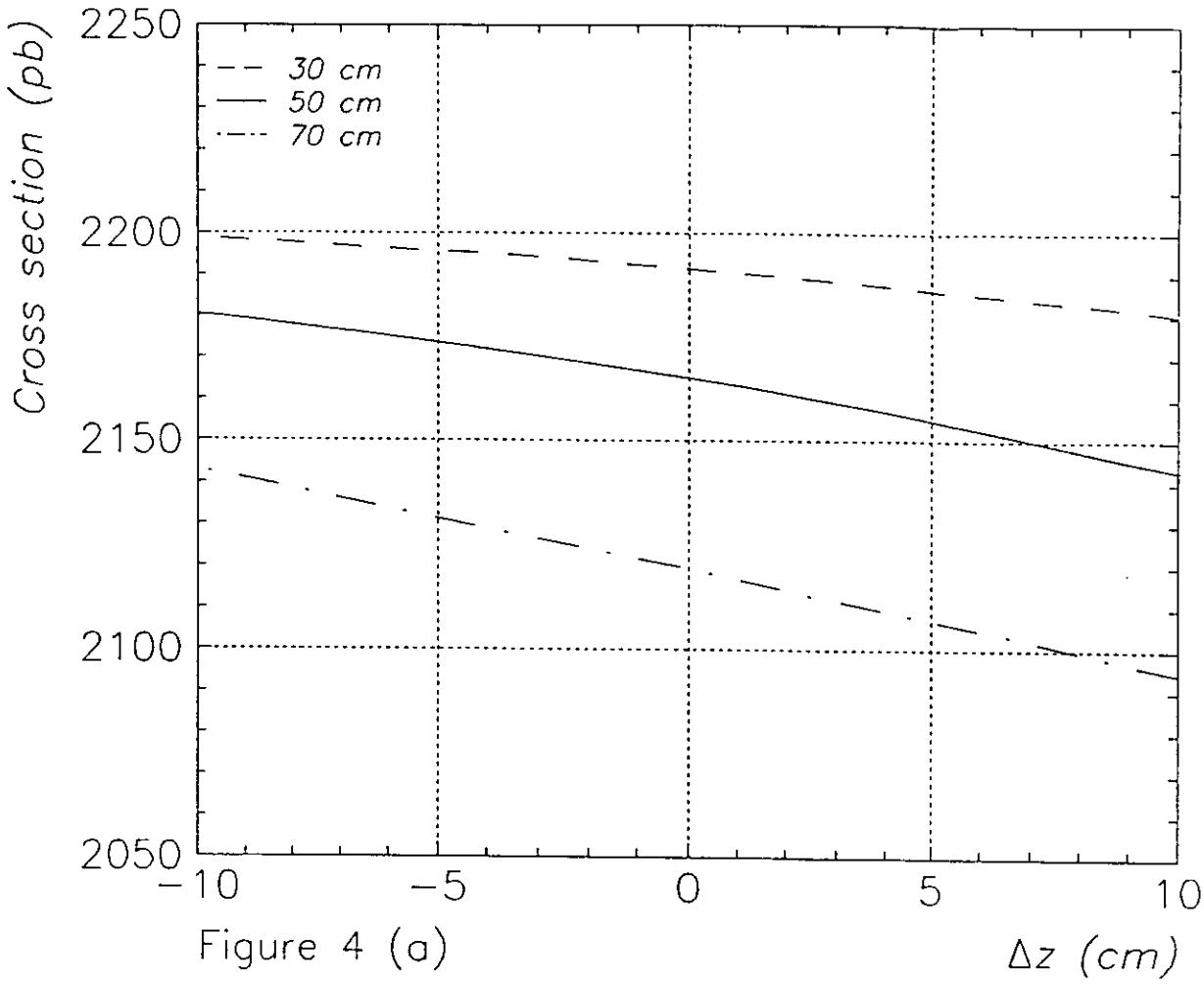

Figure 4 (a)

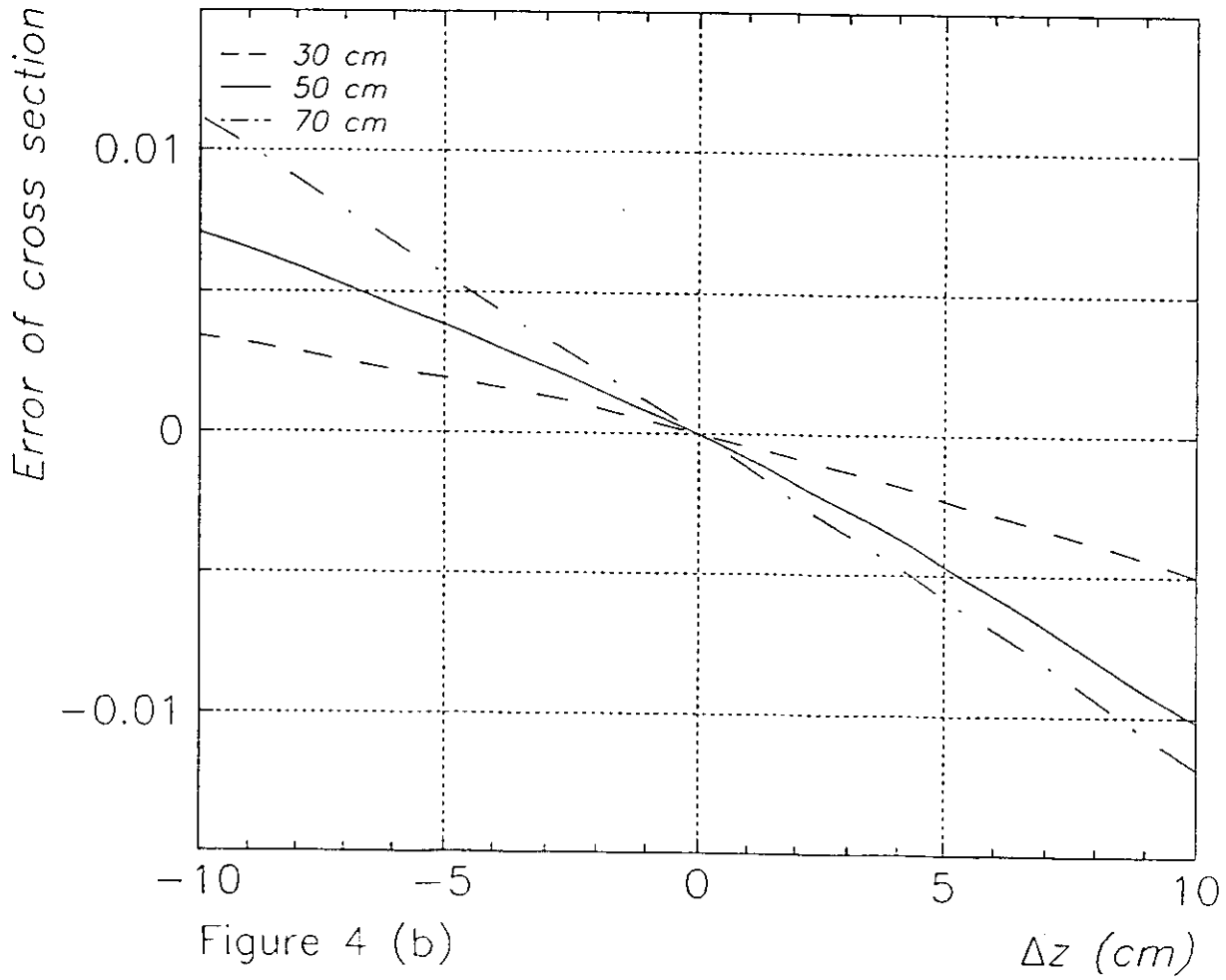

Figure 4 (b)

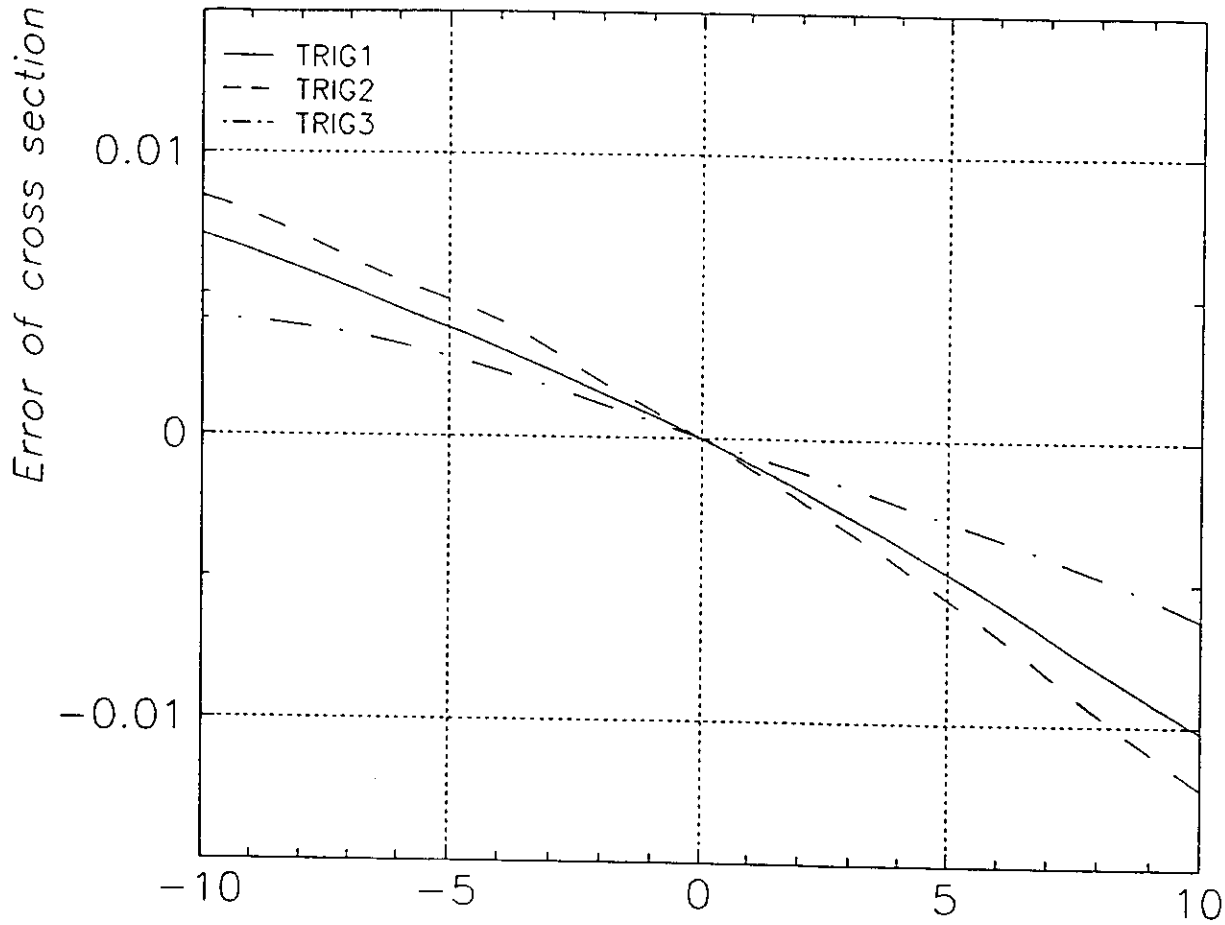

Figure 5 (a)

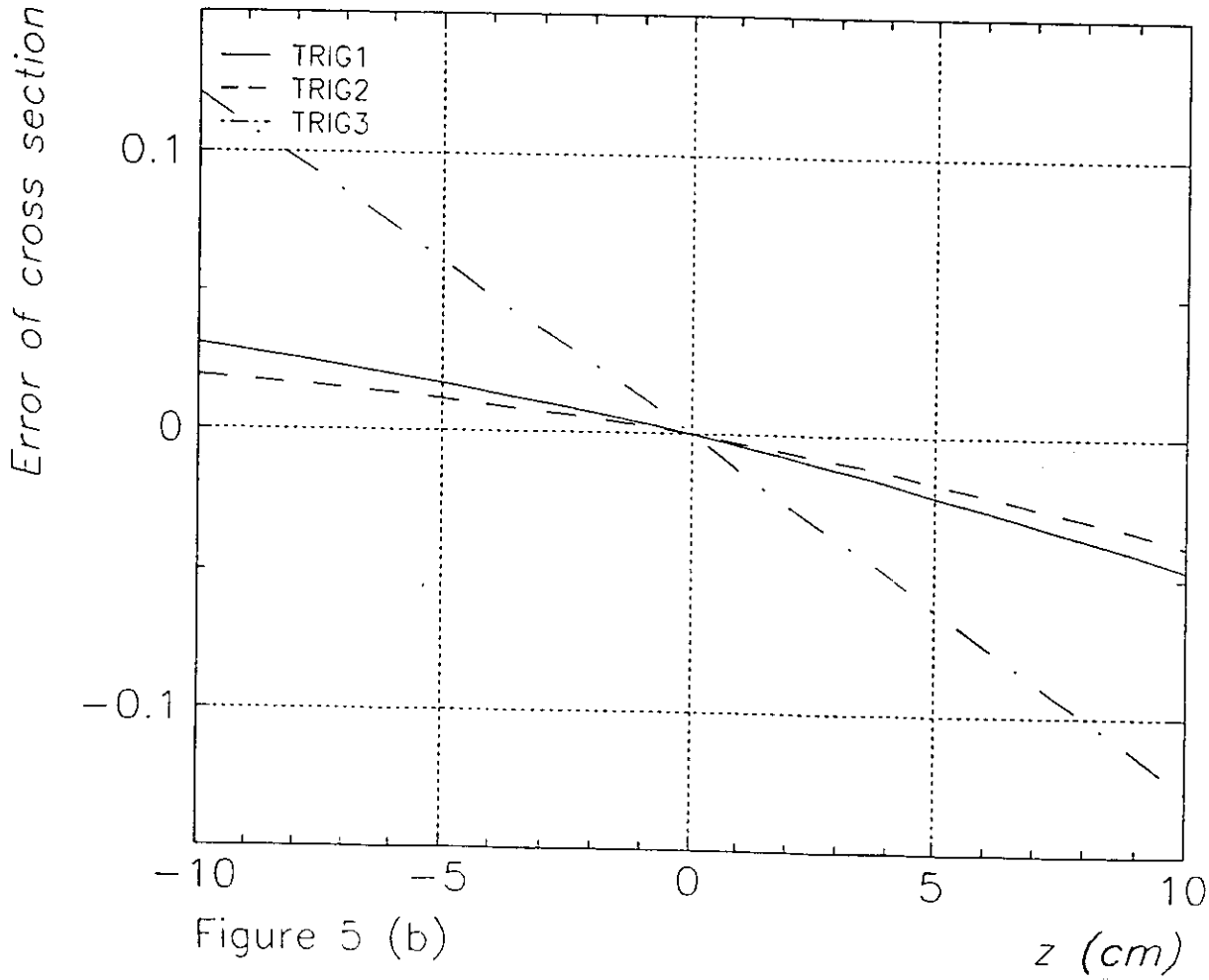

Figure 5 (b)

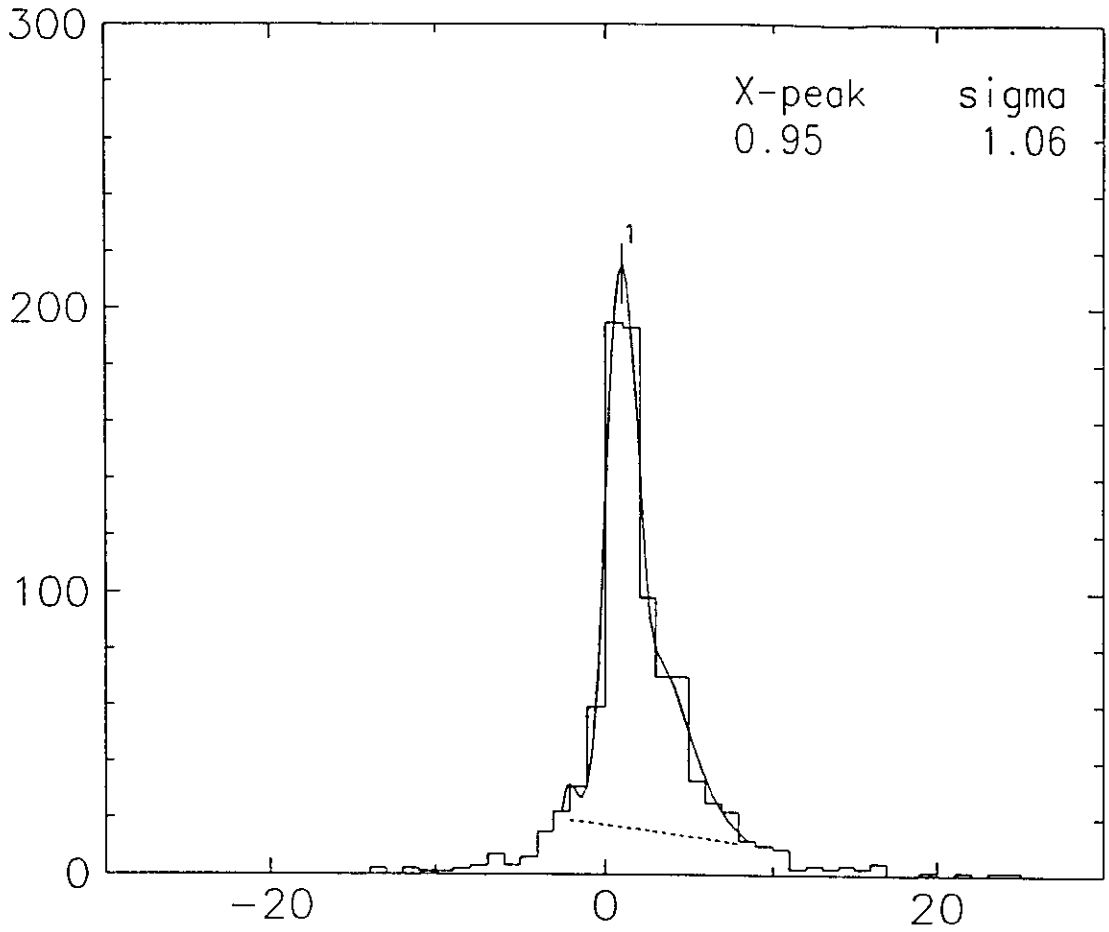

Figure 6 (a)

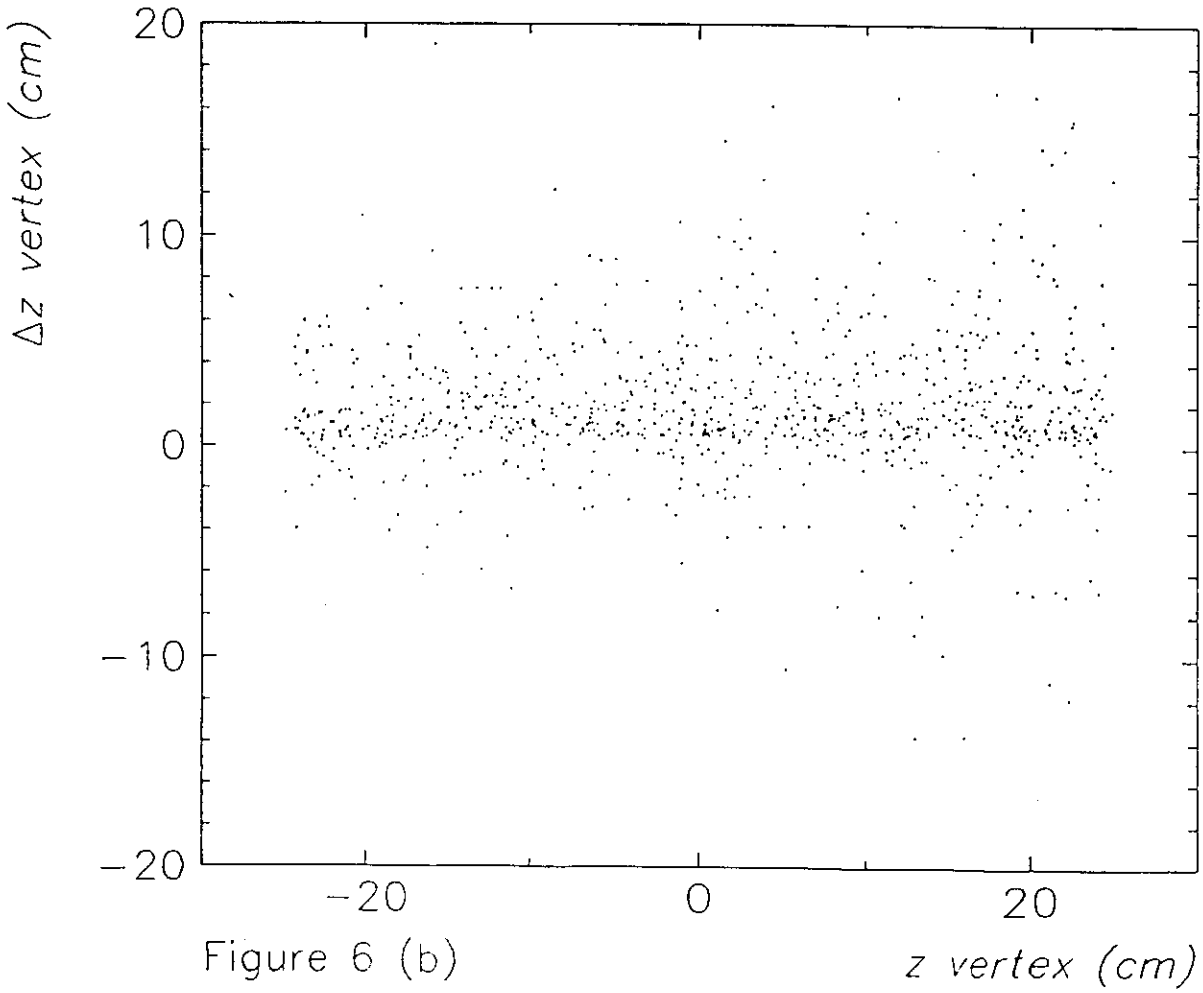

Figure 6 (b)

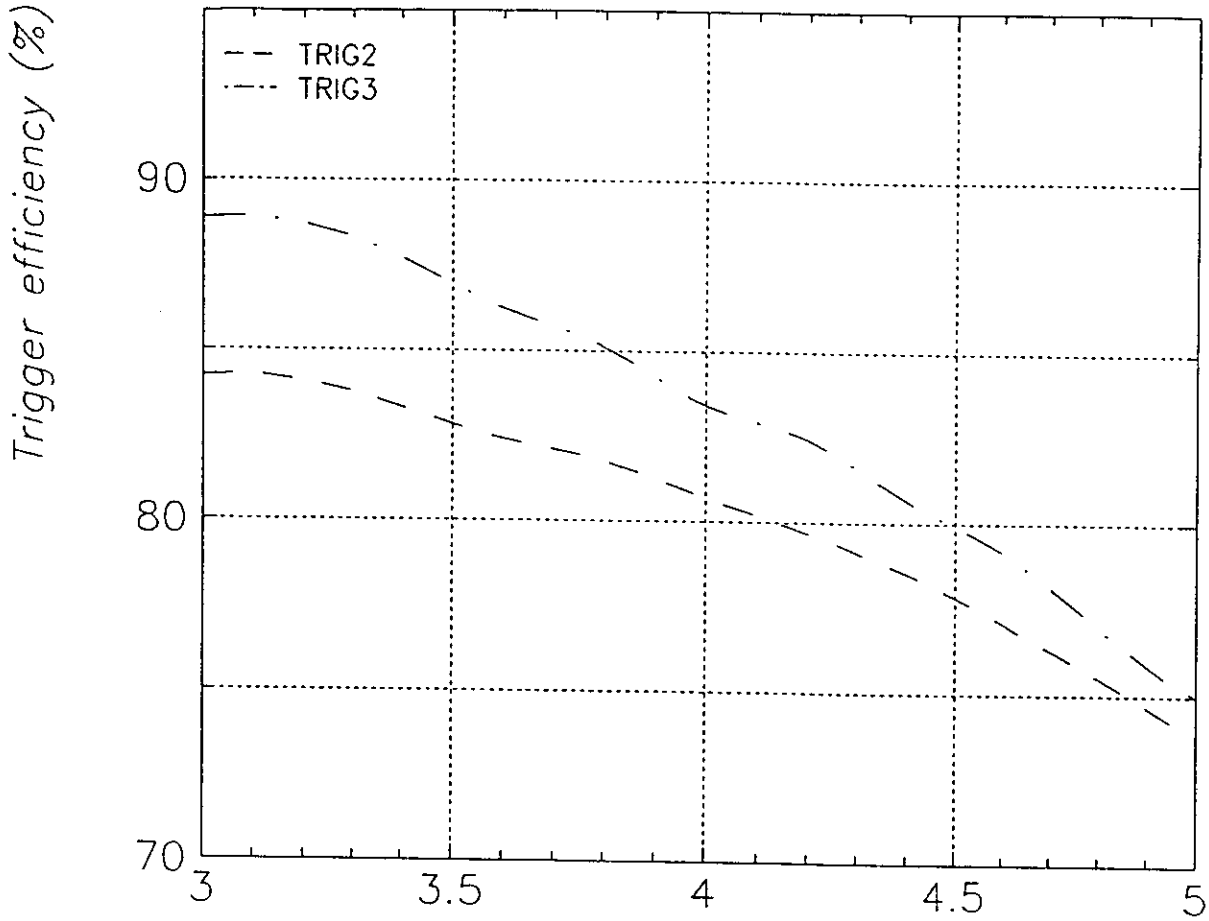

Figure 7 (a)

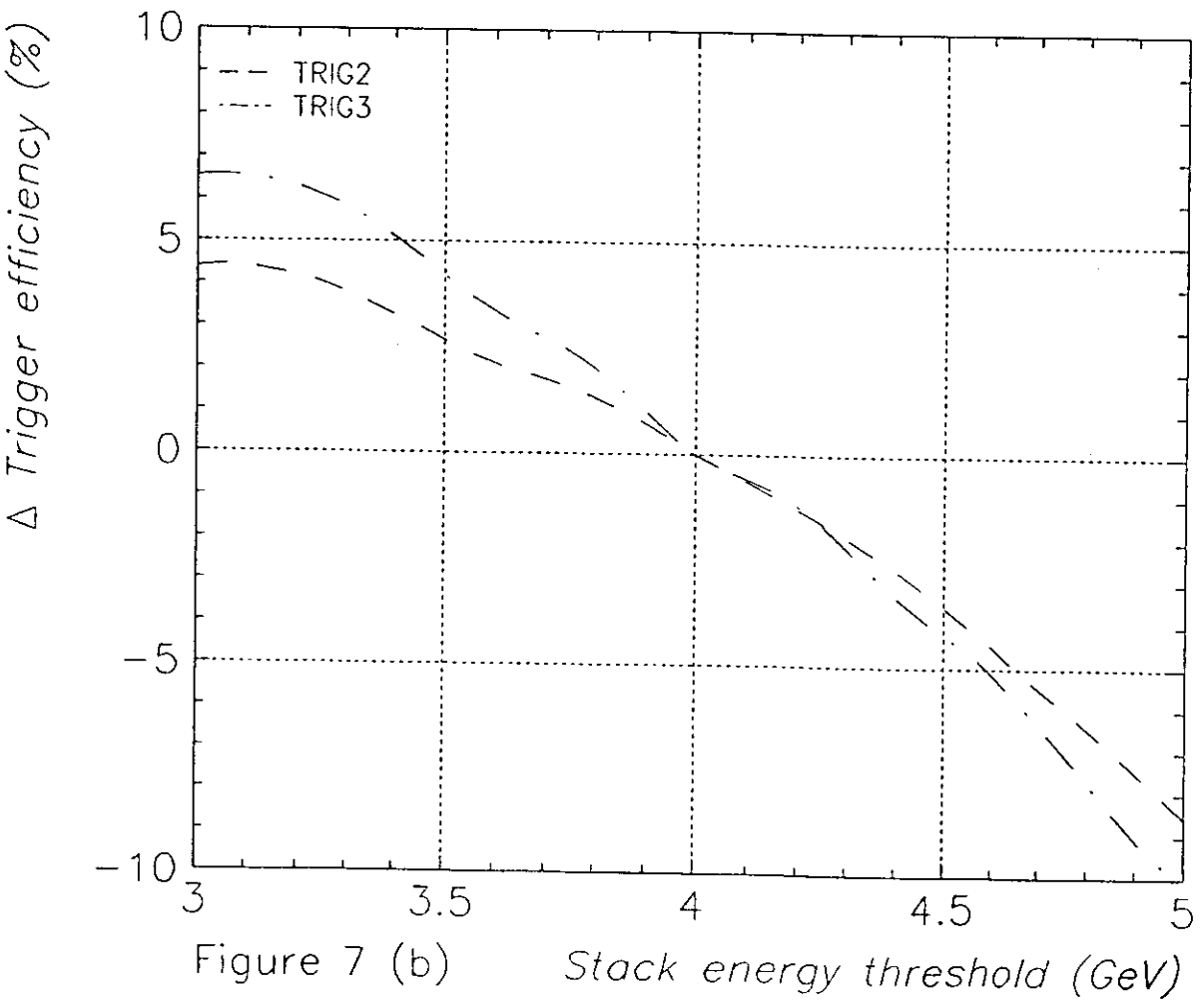

Figure 7 (b)